Journal of Materials Chemistry C

ROYAL SOCIETY OF CHEMISTRY

PAPER

View Article Online
View Journal | View Issue

Cite this: *J. Mater. Chem. C*, 2024, **12**, 4005

Crystallization kinetics of semiconducting poly(2,5-bis(3-alkylthiophen-2-yl)-thieno-[3,2-*b*]thiophene) (PBTTT) from its different liquid phases†

Valentina Pirela,[a] Alejandro J. Müller *[ab] and Jaime Martín *[abc]

Because the electronic properties of semiconducting polymers are inexorably linked to their solid-state microstructure, it is imperative to understand their complex crystallization processes fully. For example, poly(2,5-bis(3-alkylthiophen-2-yl)-thieno-[3,2-*b*]thiophene) (PBTTT), which is frequently considered a model system for highly ordered semicrystalline semiconducting polymers, can exhibit two distinct semicrystalline thin film morphologies: the so-called terrace-phase, which features high charge carrier mobility (>1 $cm^2\ V^{-1}\ s^{-1}$), and the ribbon-phase with much poorer properties. The achievement of one or the other depends on the temperature at which the polymer is thermally annealed. Our results evidence that PBTTT is in the liquid state at those "annealing temperatures" and, therefore, the achievement of the terrace- or ribbon phases depends, in fact, on the distinct structural configuration of liquid PBTTT chains at each temperature (before crystallization). Motivated by this observation, we investigate the complex crystallization kinetics of spun cast PBTTT thin films crystallized from those liquid states. We achieve this using a methodology that combines fast scanning calorimetry, X-ray scattering, and optical microscopy. We demonstrate that a preexisting smectic order enhances crystal nucleation rate, speeding up the crystallization kinetics at the early stages of phase transformation. More interestingly, our analysis reveals a complex crystallization kinetics in PBTTT, which differs from the typical crystallization behavior of commodity polymers. These results evidence that the crystallization of semiconducting polymers occurs quite differently to that of most commodity polymers, highlighting (once again) the necessity to conduct more fundamental investigations on the structure development of this important class of polymers.

Received 21st October 2023,
Accepted 16th February 2024

DOI: 10.1039/d3tc03850e

rsc.li/materials-c

Introduction

Conjugated polymers possessing semiconducting traits have great potential for a wide range of applications in the field of organic electronics, such as thin-film transistors (TFT), organic light-emitting diodes (OLEDs), thermoelectric modules, or organic solar cells,[1–4] due to their easy processing, low weight, and mechanical flexibility.

Poly(2,5-bis(3-alkylthiophen-2-yl)-thieno-[3,2-*b*]thiophene) (PBTTT-C_{12}; hereafter termed PBTTT) is a well-studied conjugated polymer exhibiting a high degree of crystalline order at room temperature.[5–8] Upon heating, PBTTT is reported to undergo two main thermal transitions: a low-temperature transition at $T \approx 150$ °C and a high-temperature transition at $T \approx 250$ °C. Interestingly, a thermal annealing below or above the high-temperature transition permits tuning its solid-state morphology/microstructure and, more importantly, its electrical properties. For example, a crystalline ribbon-like morphology with only moderate charge carrier mobility results when PBTTT is thermally annealed above the high-temperature transition. In contrast, thermal annealing PBTTT thin films at a temperature in between low-temperature and high-temperature transitions yields a semicrystalline terrace-like morphology[5–7] that exhibits remarkable charge carrier mobilities, frequently overpassing

[a] *POLYMAT and Department of Polymers and Advanced Materials: Physics, Chemistry, and Technology, Faculty of Chemistry, University of the Basque Country UPV/EHU, Paseo Manuel de Lardizabal 3, 20018, Donostia-San Sebastián, Spain. E-mail: jaime.martin.perez@udc.es, alejandrojesus.muller@ehu.es*
[b] *IKERBASQUE, Basque Foundation for Science, Plaza Euskadi 5, 48009, Bilbao, Spain*
[c] *Universidade da Coruña, Campus Industrial de Ferrol, CITENI, Esteiro, 15471 Ferrol, Spain*

† Electronic supplementary information (ESI) available: Experimental section where the equipment, techniques, and protocols for AFM, PLOM, GIWAXS and FSC are described in detail. AFM experiments to show the morphology of the material from both ISO state and LC state are shown; GIWAXS and PLOM experiments depicting PBTTT at different temperatures; comparison of overall crystallization kinetics of PBTTT with PP; table with the values obtained from applying the Avrami theory is also provided. See DOI: **https://doi.org/10.1039/d3tc03850e**

1 cm^2 V^{-1} s^{-1}.[6,7,9,10] This suggests that the distinct structural configuration of PBTTT chains (short- and long-range molecular order, conformation, *etc.*) at the annealing temperature leads to different structural rearrangement processes in the material that, eventually, result in solid-state microstructures/morphologies with different electrical performances. However, from the vast literature on PBTTT, it is rather unclear how are the structural rearrangement processes in the material that yield the terrace- and the ribbon- morphologies. On the one hand, this is motivated by the complex thermal behaviour described above and, on the other hand, by the fact that PBTTT is known to exhibit liquid crystalline order. More specifically, it has been proposed that PBTTT can form a smectic mesophase, *i.e.*, a liquid phase where polymer chains possess orientational and a certain positional order, which results in the formation of layered structures.[11,12] Therefore, it remains unclear whether the ribbon and the terrace phases result from an actual annealing process of the semicrystalline state, in which the quality of the crystalline domains is improved (like most of the typical thermal annealing processes) or whether they result through a crystallization process from the liquid states.

According to previous works, the kinetics of the crystallization process seem to have a profound impact on the resulting solid-state microstructure. For example, Kang *et al.*[13] reported that the crystallization rate has a severe impact on the solid-state morphology and electrical properties of PBTTT crystallized from the mesophase. Employing X-ray diffraction, Vakshouri *et al.*[14] investigated how structural order developed at 100 y 150 °C. However, as they mention in the manuscript, those temperatures are above the crystallization temperature for PBTTT and were chosen to anneal the liquid-crystal state. Recently, Qu *et al.* combined Raman spectroscopy and fast scanning calorimetry (FSC) and investigated the structural evolution of PBTTT at various isothermal temperatures *via* the evolution of calorimetric peaks and Raman modes. The method is proven to be efficient, however their interpretation of the thermotropic behaviour of the polymer contradicted previous literature.[6,9,14] For example, they claim that crystallization of backbones at 140 °C, while that temperature is supposed to be above the melting temperature of crystals (according to most of the literature). Likewise, the associate an endothermic calorimetric peak showing up at ~30 °C with the melting of side chains, which, according to our data (shown later on in the manuscript) it is likely due to physical ageing of glassy material regions.

Motivated by the apparent discrepancy in the literature related to the thermotropic phase behaviour of PBTTT, in this paper, we first resolve the thermotropic phase behavior of PBTTT.[15] Then, we establish that, interestingly, both the terrace and the ribbon phases develop *via* crystallization processes from liquid states with different molecular order (a smectic liquid and an isotropic liquid). Ultimately, we study the crystallization kinetics of spun cast PBTTT thin films from those different liquid states. These results reveal a complex crystallization kinetics that deviates from the typical crystallization behavior of polymers, being more accentuated in the crystallization from the smectic liquid.

Results and discussions

We begin our study by resolving the thermotropic phase behavior of PBTTT. For that, PBTTT (M_w = 65 000; $Đ$ = 2.5) thin films (~100 nm thick) were spun cast onto the chip sensors of a Mettler Toledo Flash DSC +2 fast scanning calorimeter from chlorobenzene solutions (20 mg mL^{-1}). The thermal protocol applied is shown in Fig. 1A. PBTTT films were first heated well above the high-temperature transition, T_{LC}, (*e.g.*, 350 °C) for 1 s to erase any previous thermal history while avoiding thermal degradation of the material. Then, the material was rapidly cooled (at −4000 °C s^{-1}) to a range of isothermal temperatures (T_a) and held at those T_as for 1 h. During this time, the material had time to undergo the physical process that is relevant at that temperature, *e.g.*, crystallization, physical aging, ordering of the liquid mesophase, *etc.* Subsequently, the material was cooled at −4000 °C s^{-1} to a temperature well below the glass transition temperature, T_g, (*e.g.*, −80 °C). From there, a heating scan at 4000 °C s^{-1} was recorded up to a temperature above T_{LC} (referred to as ''analysis scan'' in Fig. 1A). Finally, the material is cooled to a temperature below T_g at −4000 °C s^{-1} and a second heating scan was recorded (also at 4000 °C s^{-1}), which will serve as a reference scan.

Fig. 1B displays the calorimetric signals resulting from the heating traces referred to as ''analysis scan'' and ''reference scan'' for each T_a applied. The corresponding T_as are shown on the right-hand side of each curve. We note that any significant difference between the analysis scans and the reference scans results from the development of a specific physical process during the isothermal step at the indicated T_a, thereby reflecting the thermal response of PBTTT at that T_a. As a result, the analysis of the differences between the ''analysis scan'' and ''reference scan'' in the whole range of T_as informs about the thermotropic phase behavior of the material.

Our data shows at least four distinct endothermic processes in the ''analysis scans'' that are absent in the ''reference scans'' (these endothermic processes are shadowed in different colors). At low T_as, from T_a = −70 °C to approximately T_a = 20–30 °C, an endotherm corresponding to the enthalpic relaxation during the devitrification can be observed (shadowed in orange). Because enthalpic relaxations are linked to the physical aging of the material during the isothermal step, it can be concluded that PBTTT is in a glassy state in the temperature region below 20–30 °C, which corresponds to the T_g of the material. Whether our data includes one or two distinct enthalpic relaxation processes is a question that needs to be investigated further.

At T_as immediately higher than T_g (T_a values ranging from 40 °C to 100 °C) PBTTT is a supercooled liquid and, therefore, it should be able to crystalize during the isothermal steps. The melting of crystals formed by cold crystallization at T_as between 40 and 100 °C resulted in sharp endothermic peaks (highlighted in purple). Hence, within this temperature range, PBTTT is semicrystalline. Temperature-resolved grazing incidence wide-angle X-ray scattering (GIWAXS) results shown in ESI† Fig. S1 support this interpretation as it clearly demonstrates that the crystallization of PBTTT progresses at 80 °C (the

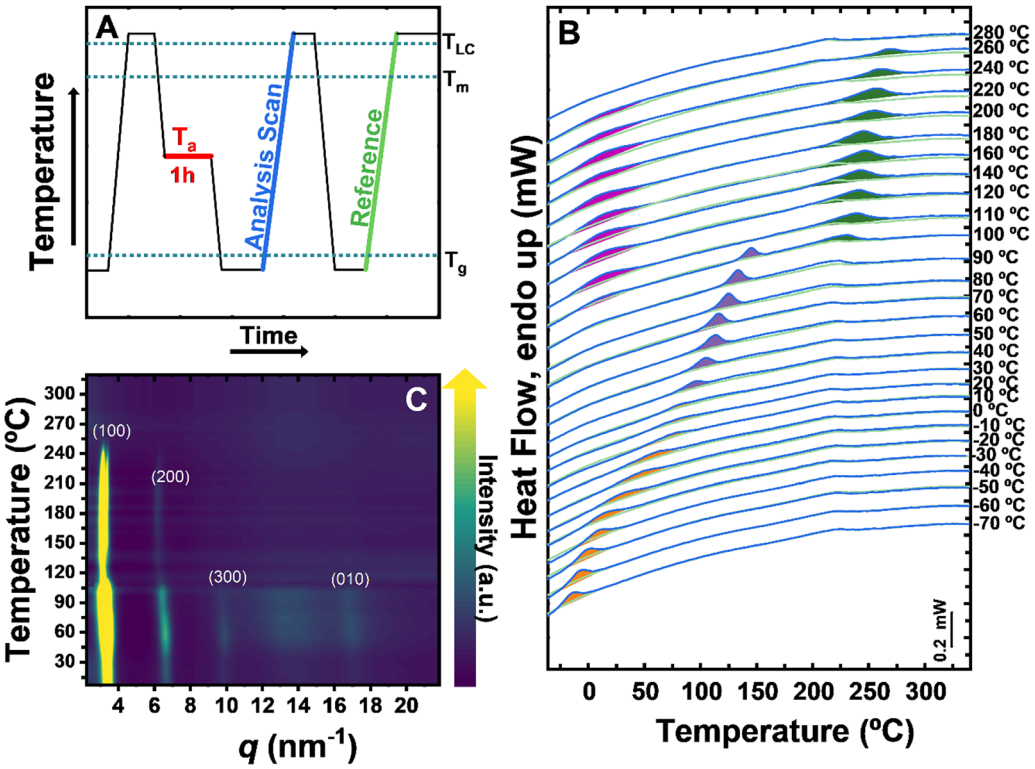

Fig. 1 (A) Thermal protocol employed for the experiments. (B) FSC heating traces referred to as "analysis scans" and "reference scans" in A (conducted at 4000 °C s^{-1}). Endothermic peaks are highlighted in orange, purple, pink and green. (C) Temperature-resolved *in situ* grazing incidence wide-angle X-ray scattering (GIWAXS) data during heating.

intensity of the (*hk*0) and the (010) peaks increase and a new peak centered at $q \approx 16$ nm^{-1} appears), which is incompatible with PBTTT being below T_g at that temperature. Interestingly, the area of the crystal melting endotherm in Fig. 1B increases until it reaches a maximum at around $T_a = 80$ °C, which corresponds to the T_a at which the crystallization develops faster.

We associate the endothermic peak located at $T \approx 250$ °C (shadowed in green) with the order–disorder transition of the liquid, *i.e.*, to the smectic-to-isotropic transition. Therefore, within the T_a range where this peak is visible in Fig. 1B (*i.e.*, between $T_a = 110$ °C and $T_a = 260$ °C), the thermodynamically stable phase in PBTTT is the liquid crystalline smectic mesophase. Above $T_a = 260$ °C; therefore, PBTTT is in the disordered liquid state or isotropic state. It should be noted that this endothermic peak (at $T \approx 250$ °C) has often been associated with the melting of crystals, and therefore, PBTTT has been considered to be in the semicrystalline below 250 °C. However, our data evidences that PBTTT is a liquid (crystal) between $T_a \approx 120$ °C and $T \approx 250$ °C. For example, temperature-resolved GIWAXS experiments shown in Fig. 1C and in ESI† Fig. S2 reveal no (010) peak, thereby π–π stacking, at temperatures higher than ≈120 °C. Moreover, the optical microscopy experiments included in Fig. S3 and S4 of the ESI† suggest that PBTTT is a flowable birefringent liquid at 200 °C, while it is a rigid solid at 100 °C.

Lastly, we also found deviations in the "analysis scans" with respect to "reference scans" in the temperature region between 50 and 100 °C when T_as between 100 °C and 260°C where applied, *i.e.*, when PBTTT was annealed at temperatures where the smectic mesophase is formed. While it cannot be ruled out the possibility that this broad endothermic overshoot results from the melting of side-chain crystals as it has been previously reported, we are more inclined to associate this signal with the increase of the enthalpy during the devitrification of the smectic glass. This could be explained by the fact that during a certain range of annealing temperatures, some of the amorphous fraction of PBTTT undergoes physical ageing, particularly when the temperature is lowered to −80 °C, leading to an aged state in the amorphous fraction which is reflected as the low-temperature overshoot. We argue that any endothermic process showing up at such low temperatures must be related to a thermal process involving material regions that are rich in side chains. Therefore, the endothermic peak could result from two processes: the melting of crystallites formed by alkyl side chains and enthalpy relaxation from physically aged glassy domains that are rich in side chains. Our main rationales for associating this endothermic peak with the latter possibility are: (i) the peak is very broad, which is more compatible with enthalpy relaxation than with a melting peak (see *e.g.* the comparison between the orange peak and the purple peak in Fig. 1B). (ii) The little shift of the peak position with T_a is also more compatible with a glass transition process than with a melting process. (iii) Prior to the heating scan in which the endothermic peak appears, samples had been quenched at 4000 °C s^{-1}, which is expected to hinder (if not suppress) the crystallization.

The temperature-resolved GIWAXS (Gracing Incidence Wide-Angle X-ray Scattering) experiments, shown in Fig. 1C, agree well with our overall interpretation of the thermotropic behavior of PBTTT. In these experiments, spin-coated PBTTT thin films were heated from room temperature to 30 °C at 20 °C min^{-1} while, simultaneously, GIWAXS patterns were recorded (further experimental details of the experiments are included in the ESI†). The thermal history applied to samples is, therefore, different to that of the FSC experiments, but the information we obtain regarding the thermotropic phase behavior is highly complementary. Our GIWAXS data shows an overall decrease of the scattered intensity at ~120 °C, coinciding with the melting of PBTTT crystals detected by FSC (*e.g.* for a T_a = 20 °C, which is comparable to a sample being stored at room temperature, like the one analyzed in GIWAXS). Moreover, at temperatures higher than 120 °C, only the diffraction peaks associated with a layer ordering, *i.e.*, the set of (*h*00) peaks of the smectic mesophase, are visible, while the (010), associated with the π–π stacking of backbones, is missing, which also agrees with the absence of crystals. Eventually, at ~250 °C, all reflections from the mesophase disappear when PBTTT transforms into a disordered liquid.

Hence, our analysis shows that -contrary to some previously reported works- PBTTT is in a liquid state at both "annealing temperatures" applied for the achievement of the terrace and the ribbon phases. This, first of all, means that such thermal treatment cannot be considered as actual annealing processes, as there are no crystals at those temperatures. The terrace-phase semicrystalline PBTTT is achieved when samples are "annealed" at 180 °C, thereby within the temperature range where PBTTT is in the smectic mesophase. In contrast, for the achievement of the ribbon-phase, PBTTT should be "annealed" above the smectic-to-isotropic transition. A further conclusion from the above is that the formation of the semicrystalline terrace- or ribbon phases must occur *via* liquid–solid transition, *i.e.*, a crystallization processes. This is an important outcome as it means that terrace and ribbon morphologies can be further controlled/tuned *via* the experimental conditions in which crystallization occurs, *e.g.* the cooling rate.

Motivated by these findings, we then investigated the crystallization kinetics of PBTTT thin films starting from both the isotropic and the smectic liquids (a schematics of the crystallization process from each liquid state is included in Scheme S1 of the ESI†). For that, we needed to design adequate thermal protocols. Fig. 2A and B display the thermal protocols employed to investigate the crystallization kinetics from the isotropic melt and from the smectic mesophase, respectively. The former is similar to the previous section of the manuscript, but here, the length of the isothermal step (*t*) is varied from 1 to 86 400 s. In addition, T_as are limited to the range where the

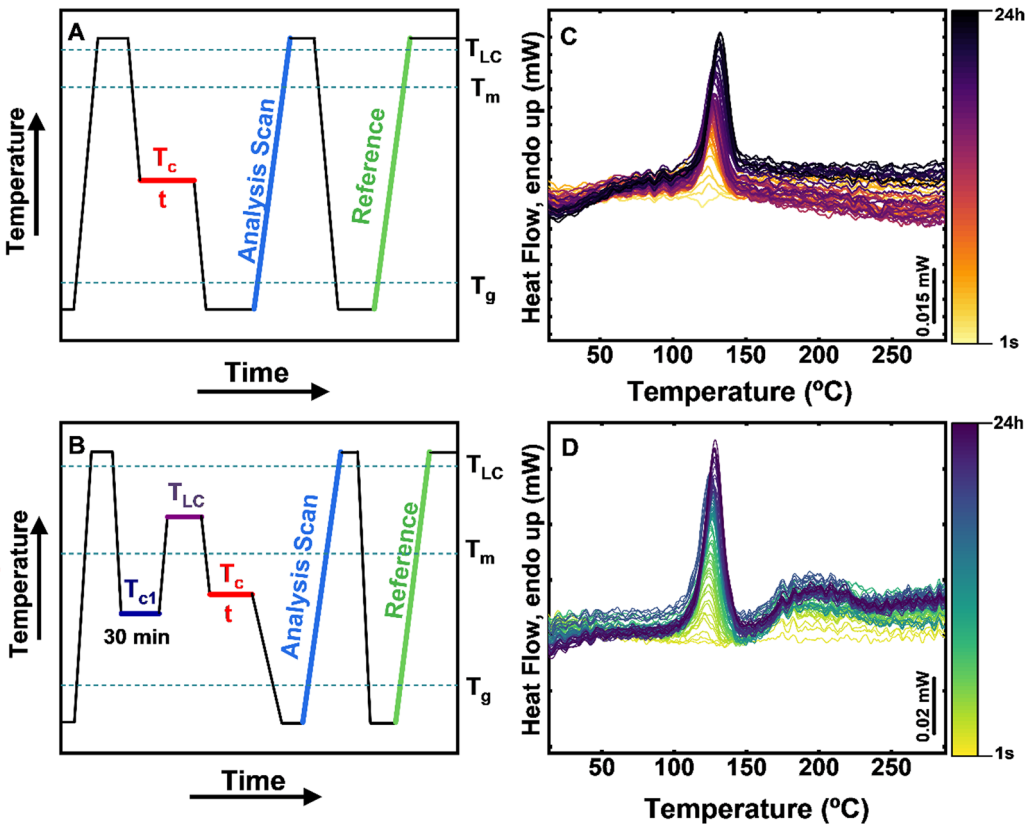

Fig. 2 (A) Thermal protocol used to study the crystallization kinetics from the disordered liquid state. (B) Thermal protocol used to study the crystallization kinetics from the smectic liquid state. (C) FSC analysis scans recorded when the thermal protocol in 2A is applied (with T_a = 80 °C) (D) FSC analysis scans recorded when the thermal protocol in 2B is applied (with T_a = 80 °C).

crystallization occurs, *i.e.*, between T_c = 60 °C and T_c = 90 °C. Hence, the analysis (heating) scans show the melting peak of the crystals isothermally formed within the time t at the selected T_c and so, the enthalpy of this peak can be used to monitor the advance of the crystallization, *i.e.*, the crystallization kinetics. We must note that the experiments shown in the previous section of the manuscript no signs of smectic mesophase when PBTTT was rapidly cooled down from 350 °C (at −4000 °C) and then annealed between T_a = 50 °C and T_a = 90 °C, indicating that no mesophase was forming prior to crystallization at those temperatures and, hence, that PBTTT can be crystallized from a completely disordered liquid state at those T_as.

The thermal protocol designed to investigate the crystallization kinetics from the smectic phase includes a first step in which the mesophase is created. We already showed that the development of the smectic mesophase occurs faster at 180 °C (the application of a T_a of 180 °C results in the most intense smectic-to-isotropic transition peak). Thus, 180 °C seems to be a suitable starting temperature for the crystallization of the smectic liquid. Moreover, preliminary studies showed that the smectic mesophase was more efficiently developed at 180 °C upon heating from the solid crystalline phase than upon cooling from the isotropic melt to avoid degradation at high temperatures over time. Therefore, the thermal protocol included an initial isothermal step at a T_c = 80 °C for 30 min in which crystals are created, followed by a further isothermal step at T = 180 °C for 1 min in which the smectic mesophase is developed. From this point on, the thermal history applied is equal to the above-mentioned protocol. Atomic force microscopy (AFM) of the thin films subject to the thermal protocols described above (shown in Fig. S5 of the ESI†) confirms the different solid-state morphologies of resulting thin films. We must note, however, that AFM data do not unarguably show that resulting morphologies (after the thermal treatment applied in FSC for the kinetics study) correspond to the terrace and the ribbon phases. It is well-known terrace and ribbon phases are better formed when films are slowly cooled down (*e.g.* 20 °C min^{-1}) from the suitable temperatures to room temperature, while here, samples are isothermically crystallized at 80 °C (after extremely fast coolings from suitable temperatures).

Fig. 2C and D show the FSC heating traces referred to as analysis scans in the protocols displayed in Fig. 2A and B, respectively. These heating traces feature the melting peak of crystals formed at T_c = 80 °C for the different crystallization times starting from the isotropic state (Fig. 2C) and the mesophase (Fig. 2D). The integration of these peaks and ulterior normalization to the integral value of the longest crystallization time (t = 24 h) yield normalized degree of crystallinity values were plotted in Fig. 3A and B. We note that the endothermic peak of the smectic-to-isotropic transition can also be seen at ∼200 °C in Fig. 2D.

Fig. 3A and B indicate that none of the PBTTT samples are able to complete their crystallization in the maximum allowed time, *i.e.*, 24 h, as the isothermal crystallization curves do not reach a saturation point. Equally striking is that the analysis evidences a complex advance of the crystallization that deviates from the typical sigmoidal curves usually obtained during the isothermal crystallization of most semi-crystalline polymers.[16,17] Plotted in a semi-log scale, curves shown in Fig. 3B display an initial sigmoidal shape (up to a ∼50% conversion) followed by an approximately linear trend. Although this behavior is observed in all curves, it is especially noteworthy for PBTTT crystallized from the LC state. We argue that this unusual behavior can occur when the crystallization process is complex and involves multiple stages.

In the crystallization process of polymers, primary nucleation occurs first, and it is immediately followed by the free growth of crystallites into semi-crystalline superstructures (*i.e.*, 1D, 2D, or 3D structures composed of crystallites separated by amorphous intervening layers). Both steps constitute the so-called primary crystallization process and typically extend over the initial 50% conversion. After primary crystallization, the semi-crystalline superstructures impinge on one another, and the secondary crystallization starts, which develops with very different kinetics than the primary crystallization. Secondary crystallization is characterized by the crystallization of part of the chains in the molten regions.

In this context, we explain the results in Fig. 3A and B by considering that the sigmoidal initial part of the isothermal curves of relative conversion *versus* time is associated with the primary crystallization process. In contrast, the second part of the kinetic curves corresponds to the secondary crystallization. Although these two crystallization stages occur in all semicrystalline polymers, both stages are partially overlapped in flexible thermoplastic materials like polyolefins, which is why the transition from the primary to the secondary crystallization occurs in succession with a smooth transition between them at approximately 50% conversion to the semi-crystalline state (see the typical behaviour, as an example, of polypropylene in Fig. S6A and a comparison with our experimental data in Fig. S6B in the ESI†).

In the case of PBTTT, a sharp transition between the first and the secondary crystallization process is clearly observed. We note, moreover, that this sharp transition is particularly noticeable when the crystallization occurs from the LC state. We argue that PBTTT chains may experience diffusion limitations during secondary crystallization by the surrounding crystallites because parts of the chains may be within neighbouring crystals or at the interphase between the crystallites and the melt. Therefore, secondary crystallization, which can also involve the re-organization and alignment of the chains within crystalline domains, is especially slow in the crystallization of a relatively rigid molecule like PBTTT, particularly when the polymer is crystallized from the smectic state. As a result, PBTTT may not be able to reach a saturation point in its crystallization process (within the time frame explored here).

To further evaluate the crystallization kinetics, experimental data was fitted to the Avrami model. We note that this model adequately describes the overall crystallization kinetics of a material that includes both the primary nuclei formation and the free growth of crystalline features until they impinge with one another (*i.e.*, until secondary crystallization begins), which

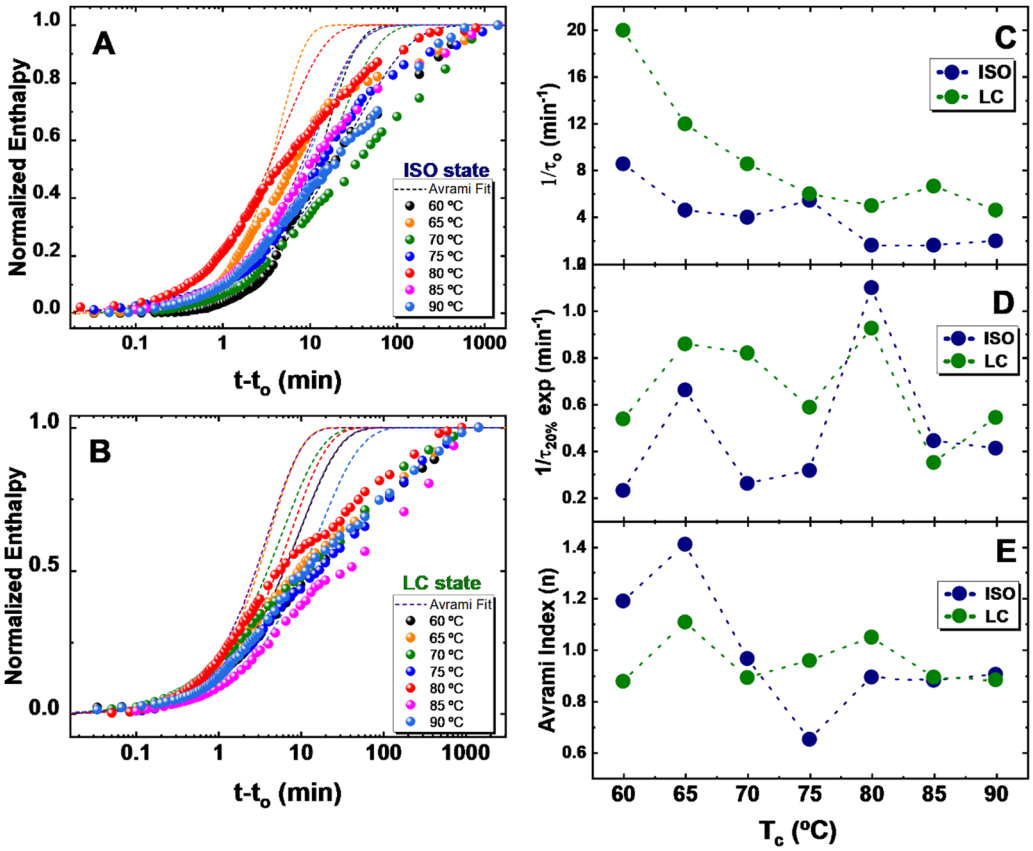

Fig. 3 Crystallization kinetics from an ISO state and from a LC state for varying times at T_c = 80 °C. (A) Advance of crystallization (from normalized enthalpy values) with time at the indicated temperatures and their corresponding Avrami fits from an ISO state. (B) Advance of crystallization (from normalized enthalpy values) with time at the indicated temperatures and their corresponding Avrami fits from a LC state. (C) Experimental values of the inverse of induction times ($1/t_o$). (D) Experimental values of the inverse of crystallization times ($1/\tau_{20\%}$). (E) Experimental values of the Avrami index (n); t and t_o are the crystallization time and the induction time, respectively.

for regular polymers typically occurs within the initial 50% of the total conversion. Therefore, fittings for large crystallization conversions tend to be, in general, inadequate, and often, as is the case for PBTTT kinetics, much lower conversions, *e.g.* of 3–20% are used to describe the kinetics within the primary crystallization range. It is noteworthy, though, that the conversion range that fits to the Avrami model is specially short for PBTTT (note the comparison with PP in Fig. S6 of the ESI†), which would also agree with a slightly different crystallization mechanism, compared to polyolefins, for example.

The model yields the expression below:[18,19]

$$1 - V_c(t - t_o) = \exp(-k(t - t_o)^n) \quad (1)$$

where V_c is the relative volumetric transformed fraction to the crystalline state, k is the overall crystallization rate constant that includes nucleation and growth components, n is the Avrami index, tis the crystallization time and t_o the induction time or the time for primary nucleation before growth has started; hence, the inverse of the induction time ($1/t_o$) is proportional to the primary nucleation rate of PBTTT, before any growth starts.

The data shown in Fig. 3C reveals that as T_c increases, the rate of primary nucleation decreases when crystallizing from both states. Interestingly, the nucleation rate is generally faster when crystallizing from a LC state than when crystallizing from an ISO state. In agreement with previous results,[15] this finding suggests that the pre-existing molecular order in the liquid crystalline state accelerates the nucleation rate, most probably because the mesophase is acting as a precursor from which primary nuclei can form.

The overall crystallization kinetics of PBTTT when crystallizing from a LC state and from an ISO state can be further examined by comparing the experimental data to the fitted results of the Avrami equation. The results obtained at a 20% conversion (conversion at which a good fitting is obtained) show that the crystallization rate ($1/\tau_{20\%}$) from a LC state is faster than when crystallizing from an ISO state at low T_cs from T_c = 60 °C to T_c = 75 °C (see Fig. 3D). Interestingly, at T_c = 80 °C the rate of crystallization suddenly increases when crystallizing from both states, with the rate of crystallization from the ISO state being the fastest. Finally, as further increases from T_c = 85 to T_c = 90 °C, the rate of crystallization becomes overall slower but similar from both states of crystallization.

The Avrami index (n) can provide information on the crystalline superstructural dimensionality and type of nucleation occurring during crystallization. Fig. 3E shows that the Avrami

index values found for PBTTT when crystallizing from both an ISO state and an LC state can be approximated to 1 (the values for all crystallization temperatures and conditions can be found in Table S1 in the ESI†). A value of n = 1 suggests the development of instantaneously nucleated needle-like crystals (or 1D structures). Although the formation of ribbon-like and terrace-like morphologies should involve different growth geometries, both are primarily formed *via* the π–π stacking of chains, which is essentially a one-dimensional process.

Conclusions

In conclusion, our results firstly evidence that it is utterly important to resolve the thermotropic phase behavior semiconducting polymers in order to advance both structure/properties interrelationships and device optimization protocols based on thermal annealing. For example, our study highlights that the ''thermal annealing'' process yielding the high-mobility terrace phase cannot be consider a proper annealing, because PBTTT is a liquid at those temperatures. Hence, we argue that the terrace-phase is formed *via* a crystallization process.

Our isothermal crystallization studies demonstrate, moreover, that the crystal nucleation rate is faster when PBTTT crystallizes from the smectic mesophase compared to the isotropic liquid phase, which agrees with our previous study on poly(9,9-di-*n*-octylfluorenyl-2,7-diyl) (PFO).[15] More interestingly, we observe a complex overall crystallization kinetics for PBTTT that differs from the general crystallization behavior of polymers, which highlights (once again) the necessity to conduct more fundamental investigations of the structure development of semiconducting polymers.

Conflicts of interest

There are no conflicts of interest from the authors to declare.

Acknowledgements

We would like to thank our colleague Dr Ricardo Pérez-Camargo for providing the Polypropylene data for comparison. We acknowledge the support of the Basque Government through grant IT1503-22. J. M. thanks MICINN/FEDER for the Ramón y Cajal contract and the grant Ref. PID2021-126243NB-I00. The Xunta de Galicia is also acknowledged for the grant Proyectos de Consolidación Ref. ED431F 2021/009.

References

1 Z. Peng, L. Ye and H. Ade, Understanding, Quantifying, and Controlling the Molecular Ordering of Semiconducting Polymers: From Novices to Experts and Amorphous to Perfect Crystals, *Mater. Horiz.*, 2022, **9**(2), 577–606.
2 A. R. Murad, A. Iraqi, S. B. Aziz, S. N. Abdullah and M. A. Brza, Conducting Polymers for Optoelectronic Devices and Organic Solar Cells: A Review, *Polymers*, 2020, **12**(11), 1–47.
3 J. A. Lim, F. Liu, S. Ferdous, M. Muthukumar and A. L. Briseno, Polymer Semiconductor Crystals, *Mater. Today*, 2010, **13**(5), 14–24.
4 Y. Furushima, A. Toda and C. Schick, Effect of Multi-Step Annealing above the Glass Transition Temperature on the Crystallization and Melting Kinetics of Semicrystalline Polymers, *Polymer*, 2020, 202.
5 I. McCulloch, M. Heeney, C. Bailey, K. Genevicius, I. MacDonald, M. Shkunov, D. Sparrowe, S. Tierney, R. Wagner, W. Zhang, M. L. Chabinyc, R. J. Kline, M. D. McGehee and M. F. Toney, Liquid-Crystalline Semiconducting Polymers with High Charge-Carrier Mobility, *Nat. Mater.*, 2006, **5**(4), 328–333.
6 D. M. Delongchamp, R. J. Kline, Y. Jung, D. S. Germack, E. K. Lin, A. J. Moad, L. J. Richter, M. F. Toney, M. Heeney and I. Mcculloch, Controlling the Orientation of Terraced Nanoscale ''Ribbons'' of a Poly(Thiophene) Semiconductor, *ACS Nano*, 2009, **3**(4), 780–787.
7 D. M. DeLongchamp, R. J. Kline, E. K. Lin, D. A. Fischer, L. J. Richter, L. A. Lucas, M. Heeney, I. McCulloch and J. E. Northrup, High Carrier Mobility Polythiophene Thin Films: Structure Determination by Experiment and Theory, *Adv. Mater.*, 2007, **19**(6), 833–837.
8 L. Zhang, H. Li, K. Zhao, T. Zhang, D. Liu, S. Wang, F. Wu, Q. Zhang and Y. Han, Improving Crystallinity and Ordering of PBTTT by Inhibiting Nematic to Smectic Phase Transition via Rapid Cooling, *Polymer*, 2022, **256**, 125178.
9 D. M. Delongchamp, R. J. Kline, Y. Jung, E. K. Lin, D. A. Fischer, D. J. Gundlach, S. K. Cotts, A. J. Moad, L. J. Richter, M. F. Toney, M. Heeney and I. McCulloch, Molecular Basis of Mesophase Ordering in a Thiophene-Based Copolymer, *Macromolecules*, 2008, **41**(15), 5709–5715.
10 I. McCulloch, M. Heeney, M. L. Chabinyc, D. DeLongchamp, R. J. Kline, M. Cölle, W. Duffy, D. Fischer, D. Gundlach, B. Hamadani, R. Hamilton, L. Richter, A. Salleo, M. Shkunov, D. Sparrowe, S. Tierney and W. Zhang, Semiconducting Thienothiophene Copolymers: Design, Synthesis, Morphology, and Performance in Thin-Film Organic Transistors, *Adv. Mater.*, 2009, **21**(10–11), 1091–1109.
11 V. Percec and M. Kawasumi, Synthesis and Characterization of a Thermotropic Nematic Liquid Crystalline Dendrimeric Polymer, *Macromolecules*, 1992, **25**(15), 3843–3850.
12 Q. Ding, D. Jehnichen, M. Göbel, M. Soccio, N. Lotti, D. Cavallo and R. Androsch, Smectic Liquid Crystal Schlieren Texture in Rapidly Cooled Poly(Butylene Naphthalate), *Eur. Polym. J.*, 2018, **101**, 90–95.
13 E. S. H. Kang and E. Kim, Effect of Non-Isothermal Recrystallization on Microstructure and Transport in Poly(Thieno-Thiophene)Thin Films, *Org. Electron.*, 2011, **12**(10), 1649–1656.
14 K. Vakhshouri and E. D. Gomez, Effect of Crystallization Kinetics on Microstructure and Charge Transport of Polythiophenes, *Macromol. Rapid Commun.*, 2012, **33**(24), 2133–2137.
15 V. Pirela, M. Campoy-Quiles, A. J. Müller and J. Martín, Unraveling the Influence of the Preexisting Molecular Order on the Crystallization of Semiconducting Semicrystalline Poly(9,9-Di-n-Octylfluorenyl-2,7-Diyl) (PFO), *Chem. Mater.*, 2022, **34**(23), 10744–10751.

16 in Conjugated Polymers, ed. G. Strobl, *The Physics of Polymers: Concepts for Understanding Their Structures and Behavior*, Springer, Berlin, Heidelberg, 2007, pp. 287–312.
17 E. Piorkowska and G. C. Rutledge, *Handbook of Polymer Crystallization*, John Wiley & Sons, 2013.
18 A. T. Lorenzo, M. L. Arnal, J. Albuerne and A. J. Müller, DSC Isothermal Polymer Crystallization Kinetics Measurements and the Use of the Avrami Equation to Fit the Data: Guidelines to Avoid Common Problems, *Polym. Test.*, 2007, **26**(2), 222–231.
19 R. A. Pérez-Camargo, G. M. Liu, D. J. Wang and A. J. Müller, Experimental and Data Fitting Guidelines for the Determination of Polymer Crystallization Kinetics, *Chin. J. Polym. Sci.*, 2022, **40**(6), 658–691.

